

# Spin-orbit torque-induced switching of in-plane magnetized elliptic nanodot arrays with various easy-axis directions measured by differential planar Hall resistance


著者	Yu Takahashi, Yutaro Takeuchi, Chaoliang Zhang, Butsurin Jinnai, Shunsuke Fukami, Hideo Ohno
journal or publication title	Applied Physics Letters
volume	114
number	1
page range	012410
year	2019-01-11
URL	<a href="http://hdl.handle.net/10097/00128369">http://hdl.handle.net/10097/00128369</a>

doi: 10.1063/1.5075542

# Spin-orbit torque-induced switching of in-plane magnetized elliptic nanodot arrays with various easy-axis directions measured by differential planar Hall resistance

Cite as: Appl. Phys. Lett. **114**, 012410 (2019); <https://doi.org/10.1063/1.5075542>

Submitted: 23 October 2018 . Accepted: 26 December 2018 . Published Online: 11 January 2019

Yu Takahashi, Yutaro Takeuchi, Chaoliang Zhang, Butsurin Jinnai , Shunsuke Fukami, and Hideo Ohno



View Online



Export Citation



CrossMark

## ARTICLES YOU MAY BE INTERESTED IN

[Field-free spin-orbit torque switching of a perpendicular ferromagnet with Dzyaloshinskii-Moriya interaction](#)

Applied Physics Letters **114**, 022401 (2019); <https://doi.org/10.1063/1.5052194>

[Spin-orbit-torque-driven multilevel switching in Ta/CoFeB/MgO structures without initialization](#)

Applied Physics Letters **114**, 042401 (2019); <https://doi.org/10.1063/1.5079313>

[Spin-orbit torques in high-resistivity-W/CoFeB/MgO](#)

Applied Physics Letters **112**, 192408 (2018); <https://doi.org/10.1063/1.5027855>

Lock-in Amplifiers  
up to 600 MHz



Watch



# Spin-orbit torque-induced switching of in-plane magnetized elliptic nanodot arrays with various easy-axis directions measured by differential planar Hall resistance

Cite as: Appl. Phys. Lett. **114**, 012410 (2019); doi: [10.1063/1.5075542](https://doi.org/10.1063/1.5075542)

Submitted: 23 October 2018 · Accepted: 26 December 2018 · Published Online: 11 January 2019




View Online



Export Citation



CrossMark

Yu Takahashi,<sup>1</sup> Yutaro Takeuchi,<sup>1</sup> Chaoliang Zhang,<sup>1,2,3,4</sup> Butsurin Jinnai,<sup>2</sup>  Shunsuke Fukami,<sup>1,2,4,5,6,7,a)</sup> and Hideo Ohno<sup>1,2,4,5,6,7</sup>

## AFFILIATIONS

<sup>1</sup> Laboratory for Nanoelectronics and Spintronics, Research Institute of Electrical Communication, Tohoku University, Sendai 980-8577, Japan

<sup>2</sup> Center for Spintronics Integrated Systems, Tohoku University, Sendai 980-8577, Japan

<sup>3</sup> Frontier Research Institute for Interdisciplinary Science, Tohoku University, Sendai 980-8578, Japan

<sup>4</sup> Center for Innovative Integrated Electronic Systems, Tohoku University, Sendai 980-0845, Japan

<sup>5</sup> Center for Spintronics Research Network, Tohoku University, Sendai 980-8577, Japan

<sup>6</sup> Center for Science and Innovation in Spintronics (Core Research Cluster), Tohoku University, Sendai 980-8577, Japan

<sup>7</sup> WPI-Advanced Institute for Materials Research, Tohoku University, Sendai 980-8577, Japan

<sup>a)</sup> Author to whom correspondence should be addressed: [s-fukami@riec.tohoku.ac.jp](mailto:s-fukami@riec.tohoku.ac.jp).

## ABSTRACT

Spin-orbit torque-induced switching of an elliptical nanomagnet with an in-plane easy axis allows sub-ns and field-free operation. Since its properties crucially depend on the design of the nanomagnet such as the easy-axis direction, it is of high importance to systematically elucidate the dependence of performance on various parameters of the nanomagnet towards magnetoresistive random access memory applications. Here, we show a scheme to statistically evaluate the switching properties of in-plane nanomagnets in a short turnaround time. We use devices with an array of CoFeB/MgO nanomagnets formed on a cross-shaped Ta/W Hall bar, and the differential planar Hall resistance is measured to study the magnetization switching. Using the scheme, we investigate the easy-axis angle dependence of switching properties at zero magnetic fields for various current pulse widths from 100 ms to 1.7 ns. We show that the dependence of threshold switching current on the easy-axis direction significantly varies with the pulse width.

Published under license by AIP Publishing. <https://doi.org/10.1063/1.5075542>

In-plane current applied to heavy-metal/ferromagnet/oxide heterostructures generates spin accumulation in the ferromagnet due to spin-orbit interactions, which exerts torques, i.e., spin-orbit torques (SOTs), and achieves magnetization switching.<sup>1-3</sup> The SOT induced switching has attracted great attention as a new writing method of magnetoresistive random access memories (MRAMs).<sup>4-6</sup> The switching scheme can be classified into three types which are different in the direction of the magnetic easy axis with respect to the current direction. Assuming that a current is applied along the  $x$  direction and the film normal is in the  $z$  direction, the three types have the easy

axis along the  $z$ ,<sup>1</sup>  $y$ ,<sup>2</sup> and  $x$ <sup>3</sup> directions (Type Z, Type Y, and Type X, respectively, hereafter). The switching properties are expected to crucially depend on the type. Switching of Type Y is driven by the accumulated spins whose direction is collinear with the magnetization and can be described by a model of conventional spin-transfer torque (STT) switching. Therefore, the switching takes place at zero magnetic fields, and threshold switching current is inversely proportional to the pulse width in a short-pulse (precessional) regime.<sup>7</sup> On the other hand, a switching of Type Z and Type X is driven by spins which are orthogonal to the magnetization. In this case, the switching

current is insensitive to the pulse width,<sup>4,8–10</sup> but the switching direction is not determined unless the rotational symmetry of SOT is broken, for example, by applying an external field<sup>1,2,11</sup> or an exchange-bias field.<sup>12–15</sup> A previous experimental study showed that the pulse width dependence of the switching current indeed contrasts between Type X and Type Y schemes, and Type X achieves a switching in the sub-ns region with a small current density,  $1.9 \times 10^{11}$  A/m<sup>2</sup>, using a Ta/W/CoFeB/MgO stack.<sup>4</sup> In addition, the study revealed that the necessity of the external field in the Type X scheme is eliminated by canting the easy-axis direction in the film plane, showing promise for realizing field-free and high-speed SOT-MRAMs.<sup>4</sup> In this context, in-depth investigation of the dependence of switching properties on various parameters of the in-plane nanomagnet is of high importance.

Understanding of the dependence of performance on the design of devices always requires a scheme that allows systematic and statistical evaluation of device properties in short turn-around time (TAT). For nanoscale spintronic devices, in general, one can utilize a tunneling magnetoresistance (TMR) effect or a Hall effect to electrically characterize the magnetization switching. The TMR effect allows us to identify the magnetization direction by measuring the tunneling resistance of the magnetic tunnel junction (MTJ),<sup>2–4,6,7,16–19</sup> which inevitably requires relatively long TAT for SOT devices. On the other hand, measurements based on Hall effects require a relatively simple device structure, allowing short TAT. However, while the anomalous Hall effect can distinguish up and down magnetization states in perpendicular-easy-axis systems,<sup>1,9–15</sup> the planar Hall effect (PHE), which gives rise to a variation of Hall resistance with the in-plane magnetization direction, cannot distinguish 180° switching of in-plane magnets by just measuring the Hall resistance due to its twofold symmetry. Recently, a method was shown to overcome this issue, where a differential planar Hall resistance is measured under off-axis bidirectional magnetic fields for a Type Y structure with a single elliptic nanodot.<sup>20</sup> However, the developed scheme requires well-controlled sample fabrication processes to obtain sufficient signal-to-noise ratios (S/N), eventually making TAT long, as discussed later.

Here, we show a scheme to statistically examine the switching properties of in-plane nanomagnets with large S/N based on the differential planar Hall resistance measurement. The developed scheme uses a sample that can be prepared with a short TAT, allowing systematic investigation. Using this scheme, we study the easy-axis angle dependence of switching current as a function of pulse width for a Ta/W/CoFeB/MgO stack.

The stack, Ta (7 nm)/W (1.6 nm)/CoFeB (1.68 nm)/MgO (1.6 nm)/Ta (1 nm) [Fig. 1(a)], is deposited on a highly resistive Si substrate by dc/rf magnetron sputtering. The easy axis of the CoFeB layer with this thickness is confirmed to be in the film plane from vibrating sample magnetometry. After the deposition, CoFeB/MgO/Ta layers are patterned into an array of elliptic nanodots by electron-beam (EB) lithography and Ar ion milling. Subsequently, Ta/W layers are patterned into a microscale Hall bar by photolithography and Ar ion milling. Finally, Cr (5 nm)/Au (100 nm) electrodes are formed at the ends of the channel and Hall probes by photolithography and lift-off. The

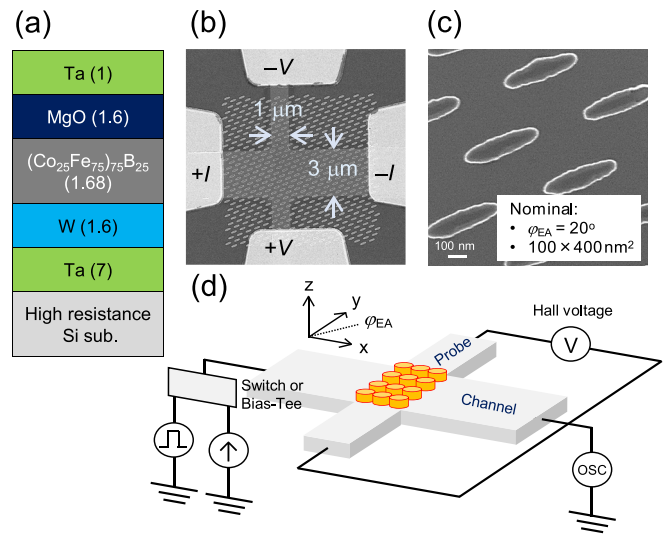


**FIG. 1.** (a) Film stack used in this study. SEM images of (b) fabricated sample and (c) nanodot array. (d) A schematic of the measurement configuration.

processed wafers are annealed at 300 °C for an hour. All the devices with various easy-axis angles  $\varphi_{EA}$  are prepared simultaneously on the same Si wafer. Note that the magnetic anisotropy is independent of  $\varphi_{EA}$  (see supplementary material). Figures 1(b) and 1(c) show scanning electron microscopy (SEM) images of a fabricated sample containing nanodots with a nominal size of  $100 \times 400$  nm<sup>2</sup> and  $\varphi_{EA} = 20^\circ$ . Widths of the channel and the Hall probe are 3 and 1  $\mu\text{m}$ , respectively. The direction of magnetization in nanodots at the cross of the channel and the probe can be detected via Hall resistance. An area of the nanodot array is greater than that of the Hall cross so that fine-controlled mask alignment during lithography steps is not required between each mask layer, while providing large S/N and statistical information because of the number of nanomagnetic dots, in contrast to the previous study.<sup>20</sup> Accordingly, this structure can be fabricated with much shorter TAT than the devices for the TMR measurement and those with a single nanodot for the PHE measurement.<sup>20</sup> Neighboring nanodots are separated with a long enough distance to suppress the dipolar field acting upon the nearest dots by less than one tenth of the switching field.<sup>21</sup> A schematic diagram for the measurement setup is shown in Fig. 1(d). We measure the Hall voltage with a 100  $\mu\text{A}$  read current under off-axis bidirectional fields, as detailed later, to identify the magnetization state.

We first describe the measurement method to detect SOT switching using PHE. We define  $\varphi_M$  as the angle of the magnetization from the x direction, i.e., the channel current direction, in the film plane. Then, the planar Hall resistance  $R_{PHE}$  is described as

$$R_{PHE} = \frac{kM_{||}^2}{t} \sin 2\varphi_M, \quad (1)$$

where  $k$  is a constant depending on the material,  $M_{||}$  the in-plane component of the magnetization, and  $t$  the thickness of the magnetic layer. Figure 2(a) shows the measured  $R_{PHE}$  under a

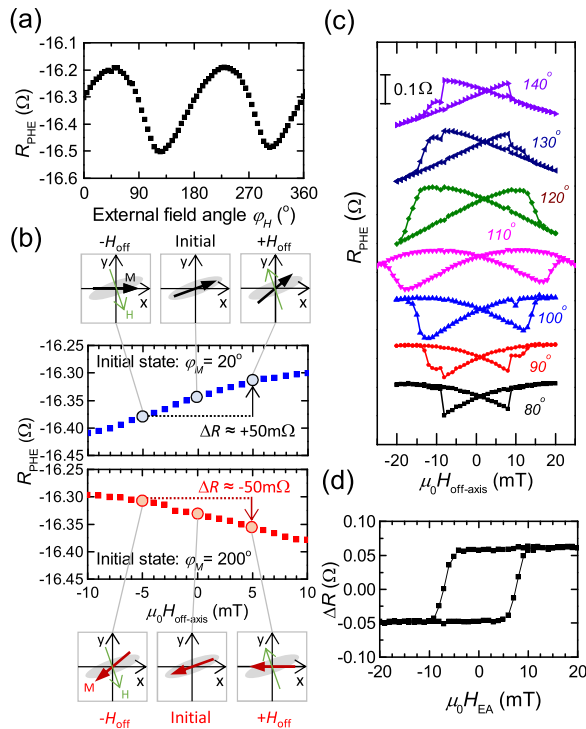


**FIG. 2.** (a) In-plane field angle  $\varphi_H$  dependence of  $R_{\text{PHE}}$ . The magnitude of the applied field is 100 mT. (b) Off-axis field  $H_{\text{off-axis}}$  dependence of  $R_{\text{PHE}}$  with different initial states and the schematics of magnetic states under  $H_{\text{off-axis}}$ . (c)  $H_{\text{off-axis}}$  dependence of  $R_{\text{PHE}}$ , where  $H_{\text{off-axis}}$  is applied along various angles  $\varphi_H$ . (d) Differential Hall resistance  $\Delta R$  between  $R_{\text{PHE}}$  at  $\mu_0 H_{\text{off-axis}} = \pm 5$  mT along  $\varphi_H = 100^\circ$  as a function of magnetic field along the easy-axis direction. (a)–(d) are the results for a typical device structure ( $100 \times 400 \text{ nm}^2$  and  $\varphi_{\text{EA}} = 20^\circ$ ).

rotated in-plane field with the angle  $\varphi_H$  from  $0^\circ$  to  $360^\circ$ . The curve is distorted from the  $\sin 2\varphi_H$  function due to the shape anisotropy of elliptic nanodots. Next, we describe how to examine magnetization switching by taking a case of  $\varphi_{\text{EA}} = 20^\circ$  as an example. The magnetization switching is detected by measuring  $R_{\text{PHE}}$  while applying small off-axis bidirectional external fields, as in the previous study.<sup>20</sup> Figure 2(b) shows  $R_{\text{PHE}}$  as a function of an off-axis magnetic field along  $\varphi_H = 100^\circ$  for a sample with  $\varphi_{\text{EA}} = 20^\circ$  whose initial magnetization state is  $\varphi_M = 20^\circ$  (upper panel) or  $200^\circ$  (lower panel). For  $\varphi_M = 20^\circ$ , a small field applied along the positive (negative) direction, i.e.,  $\varphi_H = 100^\circ$  ( $\varphi_H = 280^\circ$ ), rotates the magnetization in the counterclockwise (clockwise) direction (see the schematics), resulting in an increase (a decrease) in the Hall resistance. The opposite situation arises when  $\varphi_M = 200^\circ$ . Thus, a positive (negative) differential Hall resistance  $\Delta R$  between positive and negative field applications is observed for the former (latter) case. In such a way as to measure  $\Delta R$  under bidirectional off-axis external fields, we examine magnetization switching in samples with the arbitrary easy-axis direction.

Figure 2(c) shows  $R_{\text{PHE}}$  as a function of off-axis field applied along various  $\varphi_H$  values. The resistance change increases as  $\varphi_H$  becomes closer to the hard-axis direction  $\varphi_{\text{HA}} (=110^\circ)$ . Above around 10 mT,  $R_{\text{PHE}}$  shows a discontinuous change owing to a

magnetization switching, indicating that the off-axis field to examine the magnetization direction is limited to be sufficiently smaller than 10 mT. Prior to the evaluation of SOT switching, we perform this measurement and determine the magnitude and direction of the off-axis field, where a reliable identification of the magnetization direction is possible. Figure 2(d) shows a typical  $\Delta R$  versus easy-axis field  $H_{\text{EA}}$  in the sample mentioned above, where the bidirectional off-axis field of 5 mT is applied along  $\varphi_H = 100^\circ$  after applying each  $H_{\text{EA}}$ . A typical field-driven magnetization switching is observed with sufficient S/N. A gradual change of  $\Delta R$  near the switching field reflects a dot-to-dot variation of the switching field among the nanodots on the Hall cross, providing statistical information.

Using the method described above, we then evaluate SOT switching in samples with various  $\varphi_{\text{EA}}$  values using pulsed currents with various widths  $t_p$  down to 1.7 ns, which is the shortest duration in our employed setup.  $\varphi_{\text{EA}}$  is varied from  $0^\circ$  (Type X) to  $90^\circ$  (Type Y) at  $10^\circ$  step. The nominal size of nanodots shown here is  $100 \times 400 \text{ nm}^2$ . Figure 3(a) shows  $\Delta R$  versus applied current at  $t_p = 100$  ms for samples with  $\varphi_{\text{EA}} = 0^\circ, 30^\circ, 60^\circ,$  and  $90^\circ$ . A perpendicular external field is applied only for the sample with  $\varphi_{\text{EA}} = 0^\circ$  to have a deterministic switching. Clear hysteresis loops are observed for all the samples. We define the current at which  $\Delta R$  crosses the average of all measured points of  $\Delta R$  as the threshold switching current  $I_{\text{th}}^{\text{array}}$ . Figure 3(b) shows  $I_{\text{th}}^{\text{array}}$  as a function of  $\varphi_{\text{EA}}$  in the range of  $10^\circ$ – $90^\circ$  with various  $t_p$  values down to 1.7 ns. No field is applied during the application of the

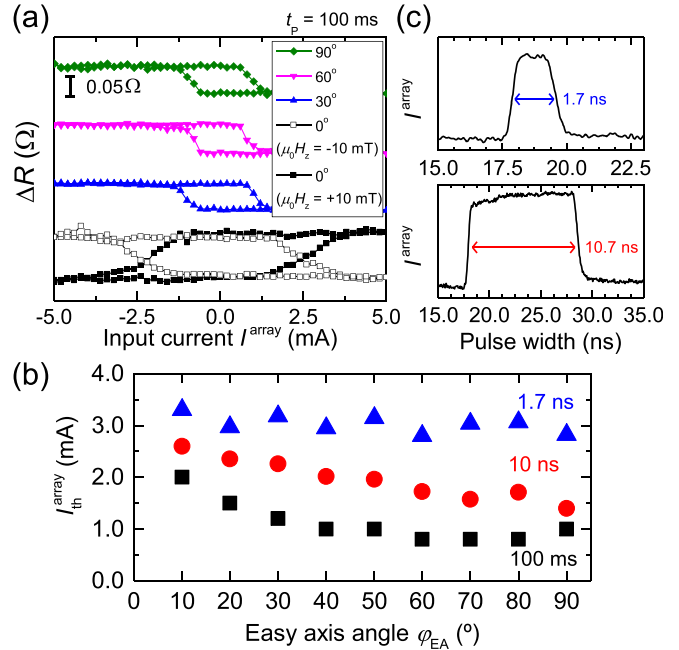


**FIG. 3.** (a)  $\Delta R$  versus applied current  $I^{\text{array}}$  loops for each easy-axis angle. (b) Easy-axis angle dependence of threshold current with various current pulse widths. (c) Transmitted current waveforms in the short pulse region. The current pulse width is measured at the point where a pulse rises up or falls down by half of the maximum amplitude.

pulsed current. Typical waveforms of the transmitted current pulse for  $t_p = 1.7$  and 10 ns are shown in Fig. 3(c). The current of 1 mA corresponds to the current density of about  $4.2 \times 10^{10}$  A/m<sup>2</sup> in the W layer, which is numerically calculated by considering the nominal structure of the Hall bar and resistivity of each layer. The switching current density hence ranges from  $2.1 \times 10^{10}$  to  $1.5 \times 10^{11}$  A/m<sup>2</sup> for various  $\varphi_{EA}$  values and current pulse widths, which are comparable with those in the previous studies using similar film stacks.<sup>4,16</sup> Besides, in consistent with the previous study,<sup>4</sup> in the longer pulse regime,  $I_{th}^{array}$  decreases with increasing  $\varphi_{EA}$ , but an increase in  $I_{th}^{array}$  with decreasing  $t_p$  for smaller  $\varphi_{EA}$  is much smaller than that for larger  $\varphi_{EA}$ . At  $t_p = 1.7$  ns,  $I_{th}^{array}$  does not significantly depend on  $\varphi_{EA}$ . In the devices, where we change the easy-axis angle while keeping the dimensions of nanomagnets the same, the magnetic properties are the same regardless of the easy-axis direction (see [supplementary material](#)). Thus, only the relative angle between the easy axis and accumulated spins should affect the switching behavior; changing the easy-axis direction can vary the balance between collinear and orthogonal components of spins accumulated in a ferromagnet layer. While the collinear spins tend to induce precession to switch the magnetization as in Type Y, the orthogonal spins drive a magnetization switching without precession as in Type X. As the magnetization goes through many precessions to switch its direction for larger  $\varphi_{EA}$  where the collinear spins dominate, the required current for switching becomes smaller in the longer pulse regime because sufficient time is provided to precess before switching. In the short-pulse regime, on the other hand, a larger current is needed to directly flip the magnetization. In contrast, for smaller  $\varphi_{EA}$  where the orthogonal spins dominate, the magnetization switching takes place without precessions, making it insensitive to the pulse width. Therefore,  $I_{th}^{array}$  depends less (much) on  $\varphi_{EA}$  in the shorter (longer) pulse regime, where the magnetization is expected to follow a similar (different) trajectory without (with or without) precessions. It is important to note that, since the channel width becomes narrower for smaller  $\varphi_{EA}$  in actual three-terminal SOT devices with a single elliptic nanomagnet, the observed trend with a virtually constant  $I_{th}^{array}$  with various  $\varphi_{EA}$  values in the employed array devices indicates that a write current of a SOT-MRAM device with a single elliptic nanomagnet becomes smaller for smaller  $\varphi_{EA}$ . As shown here, the developed scheme allows us to systematically study the SOT switching of in-plane nanomagnets as a function of various design parameters and employed materials and thus is expected to serve as a useful tool for the development of SOT-MRAM devices.

In conclusion, we show a scheme to evaluate the SOT-induced switching properties of in-plane easy-axis nanomagnets, where a differential planar Hall resistance is measured in Hall bar devices with an array of nanomagnets. This scheme offers short TAT, sufficient S/N, and statistical information of switching properties, allowing systematic investigation of SOT switching. Using the developed scheme, we evaluate the in-plane easy-axis angle dependence of the switching current for various current pulse widths. We show that switching current at zero fields decreases upon increasing the angle between the current and easy axis for the long-pulse regime, whereas at

$t_p = 1.7$  ns, it is almost constant at the same channel width. The developed scheme and obtained findings are useful for the development of SOT-MRAM devices toward high-speed and low-current operation.

See [supplementary material](#) for the evaluation of effective magnetic anisotropy fields of nanomagnets with various easy-axis directions.

We thank T. Hirata, H. Iwanuma, K. Goto, and C. Igarashi for their technical support. A portion of this work was supported by the ImpACT Program of CSTI, JST-OPERA, JSPS Core-to-Core Program, and Cooperative Research Projects of RIEC.

## REFERENCES

- <sup>1</sup>I. M. Miron, K. Garello, G. Gaudin, P.-J. Zermatten, M. V. Costache, S. Auffret, S. Bandiera, B. Rodmacq, A. Schuhl, and P. Gambardella, *Nature* **476**, 189 (2011).
- <sup>2</sup>L. Liu, C.-F. Pai, Y. Li, H. W. Tseng, D. C. Ralph, and R. A. Buhrman, *Science* **336**(6081), 555 (2012).
- <sup>3</sup>S. Fukami, T. Anekawa, C. Zhang, and H. Ohno, *Nat. Nanotechnol.* **11**, 621 (2016).
- <sup>4</sup>S. Fukami, T. Anekawa, A. Ohkawara, C. Zhang, and H. Ohno, in *IEEE Symposium on VLSI Technology*, T06-05 (IEEE, 2016).
- <sup>5</sup>S. Fukami and H. Ohno, *Jpn. J. Appl. Phys. Part 1* **56**, 0802A1 (2017).
- <sup>6</sup>K. Garello, F. Yasin, S. Couston, L. Souriau, J. Swerts, S. Rao, S. Van Beek, W. Kim, E. Liu, S. Kundu, D. Tsvetanova, N. Jossart, K. Croes, E. Grimaldi, M. Baumgartner, D. Crotti, A. Furnémont, P. Gambardella, and G. S. Kar, in *2018 Symposium on VLSI Circuits*, C08-2 (IEEE, 2018).
- <sup>7</sup>G. E. Rowlands, S. V. Aradhya, S. Shi, E. H. Yandel, J. Oh, D. C. Ralph, and R. A. Buhrman, *Appl. Phys. Lett.* **110**, 122402 (2017).
- <sup>8</sup>K.-S. Lee, S.-W. Lee, B.-C. Min, and K.-J. Lee, *Appl. Phys. Lett.* **104**, 072413 (2014).
- <sup>9</sup>C. Zhang, S. Fukami, H. Sato, F. Matsukura, and H. Ohno, *Appl. Phys. Lett.* **107**, 012401 (2015).
- <sup>10</sup>C. Zhang, S. Fukami, S. DuttaGupta, H. Sato, and H. Ohno, *Jpn. J. Appl. Phys. Part 1* **57**, 04FN02 (2018).
- <sup>11</sup>L. Liu, O. J. Lee, T. J. Gudmundsen, D. C. Ralph, and R. A. Buhrman, *Phys. Rev. Lett.* **109**, 096602 (2012).
- <sup>12</sup>S. Fukami, C. Zhang, S. DuttaGupta, A. Kurenkov, and H. Ohno, *Nat. Mater.* **15**, 535 (2016).
- <sup>13</sup>A. van den Brink, G. Vermijs, A. Solignac, J. Koo, J. T. Kohlhepp, H. J. M. Swagten, and B. Koopmans, *Nat. Commun.* **7**, 10854 (2016).
- <sup>14</sup>Y.-C. Lau, D. Betto, K. Rode, J. M. D. Coey, and P. Stamenov, *Nat. Nanotechnol.* **11**, 758 (2016).
- <sup>15</sup>Y.-W. Oh, S.-H. Chris Baek, Y. M. Kim, H. Y. Lee, K.-D. Lee, C.-G. Yang, E.-S. Park, K.-S. Lee, K.-W. Kim, G. Go, J.-R. Jeong, B.-C. Min, H.-W. Lee, K.-J. Lee, and B.-G. Park, *Nat. Nanotechnol.* **11**, 878 (2016).
- <sup>16</sup>C.-F. Pai, L. Liu, Y. Li, H. W. Tseng, D. C. Ralph, and R. A. Buhrman, *Appl. Phys. Lett.* **101**, 122404 (2012).
- <sup>17</sup>M. Yamanouchi, L. Chen, J. Kim, M. Hayashi, H. Sato, S. Fukami, S. Ikeda, F. Matsukura, and H. Ohno, *Appl. Phys. Lett.* **102**, 212408 (2013).
- <sup>18</sup>M. Cubukcu, O. Boule, M. Drouard, K. Garello, C. O. Avci, I. M. Miron, J. Langer, B. Ocker, P. Gambardella, and G. Gaudin, *Appl. Phys. Lett.* **104**, 042406 (2014).
- <sup>19</sup>T. Inokuchi, H. Yoda, Y. Kato, M. Shimizu, S. Shirotori, S. Shimomura, K. Koi, Y. Kamiguchi, H. Sugiyama, S. Oikawa, K. Ikegami, M. Ishikawa, B. Altansargai, A. Tiwari, Y. Ohsawa, Y. Saito, and A. Kurobe, *Appl. Phys. Lett.* **110**, 252404 (2017).
- <sup>20</sup>G. Mihajlović, O. Mosendz, L. Wan, N. Smith, Y. Choi, Y. Wang, and J. A. Katine, *Appl. Phys. Lett.* **109**, 192404 (2016).
- <sup>21</sup>I. Yoon and A. Raychowdhury, *IEEE Trans. Comput. Aided Des. Integr. Circuits Syst.* **37**(2), 337–349 (2018).